Shah, M. A.K.Yousaf; Lu, Yuzheng; Mushtaq, Naveed; Yousaf, Muhammad; Lund, Peter D.; Asghar, Muhammad Imran; Zhu, Bin

Designing Gadolinium-doped ceria electrolyte for low temperature electrochemical energy conversion

Published in:
International Journal of Hydrogen Energy

DOI:
10.1016/j.ijhydene.2022.12.314

Published: 30/04/2023

Document Version
Publisher's PDF, also known as Version of record

Please cite the original version:
Shah, M. A. K. Y., Lu, Y., Mushtaq, N., Yousaf, M., Lund, P. D., Asghar, M. I., & Zhu, B. (2023). Designing Gadolinium-doped ceria electrolyte for low temperature electrochemical energy conversion. *International Journal of Hydrogen Energy*, *48*(37), 14000-14011. https://doi.org/10.1016/j.ijhydene.2022.12.314

Available online at www.sciencedirect.com

ScienceDirect

journal homepage: www.elsevier.com/locate/he

Designing Gadolinium-doped ceria electrolyte for low temperature electrochemical energy conversion

M.A.K. Yousaf Shah [a,***,1], Yuzheng Lu [b,1], Naveed Mushtaq [a], Muhammad Yousaf [a], Peter D. Lund [c], Muhammad Imran Asghar [c,d,*], Bin Zhu [a,**]

[a] Jiangsu Provincial Key Laboratory of Solar Energy Science and Technology/Energy Storage Joint Research Center, School of Energy and Environment, Southeast University, No.2 Si Pai Lou, Nanjing 210096, China
[b] School of Electronic Engineering, Nanjing Xiao Zhuang University, 211171 Nanjing, China
[c] New Energy Technologies Group, Department of Applied Physics, School of Science, Aalto University, P.O. BOX 15100, FI-00076 Aalto, Finland
[d] Faculty of Physics and Electronic Science, Hubei University, Wuhan, Hubei, 430062, China

HIGHLIGHTS

- Gadolinium-doped ceria is synthesized through a wet chemical co-precipitation technique.
- The synthesized GDC electrolyte exhibits a high ionic conductivity of 0.1 S/cm at 450 °C.
- The fuel cell using the synthesized GDC produced 569 mW/cm^2 at 450 °C.
- The fuel cell device remained stable for 150 h at a high current density of 110 mA/cm^2.

GRAPHICAL ABSTRACT

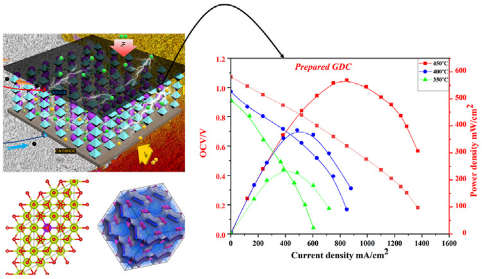

ARTICLE INFO

Article history:
Received 11 September 2022
Received in revised form
23 December 2022
Accepted 27 December 2022
Available online 10 January 2023

ABSTRACT

Reducing the operational temperature of solid oxide fuel cells (SOFC) is vital to improving their durability and lifetime. However, a traditional SOFC suffers from high ohmic and polarization losses at low temperatures, leading to poor performance. Gadolinium-doped ceria is the best ionic conductor for SOFC at lower temperatures. The present work envisages the GDC as an electrolyte for applying low-temperature solid oxide fuel cells (LT-SOFCs). So, in this regard, herein, GDC is synthesized through a wet chemical co-

---

* *Corresponding author.*
** *Corresponding author.*
*** *Corresponding author.*
E-mail addresses: alikamranshah91@seu.edu.cn (M.A.K.Y. Shah), imran.asghar@aalto.fi (M.I. Asghar), zhu-bin@seu.edu.cn (B. Zhu).
[1] These authors have contributed equally.

https://doi.org/10.1016/j.ijhydene.2022.12.314

Keywords:
Low-temperature SOFCs
High ionic conductivity
Grain-boundary conduction
Durability
High fuel cell performance

precipitation technique as a functional electrolyte layer fixed between two symmetrical porous electrodes NCAL ($Ni_{0.8}Co_{0.15}Al_{0.05}LiO_2$). Due to the improved surface properties of the synthesized GDC, particles perform better than commercially available GDC. The synthesized GDC electrolyte shows an impressive fuel cell performance of 569 mW/cm^2 and a high ionic conductivity of 0.1 S/cm at a shallow temperature of 450 °C. Moreover, the fuel cell device utilizing the synthesized GDC remained stable for 150 h of operation at a high current density of 110 mA/cm^2 at 450 °C. The high conduction mechanism has been proposed in detail. The results show that excellent fuel cell performance, high ionic conductivity, and better stability can be achieved at exceptionally low enough temperatures. Also, the proposed work suggests that new electrolytes can be designed for developing advanced low-temperature fuel cell technology.

Introduction

Solid oxide fuel cell (SOFC) enables the efficient use of multi fuels (hydrogen, methane, ammonia, hydrocarbons, etc.). In addition, a good performance without emissions can be achieved, making SOFC technology a promising future energy conversion technology [1–5]. Typically, a SOFC requires a high operating temperature to achieve adequate ionic conductivity, essential to high performance but suffers from degradation effects and poor durability. As a result of the high working temperatures (>800 °C), the fuel cell's startup and shut down cycles are lengthened, which raises the cost of and rate of degradation for the fuel cell's materials. Today, reducing the working temperature of SOFCs is a significant task, but it also comes with a substantial drawback. Reducing the operating temperature shows a considerable drop in ionic conduction and an increase in Ohmic losses. Several techniques have been devised to overcome these obstacles, such as the use of novel materials as electrolytes and the fabrication of ultra-thin electrolytes with low Ohmic resistance using thin-film technology. For example, YSZ (Yttria-stabilized zirconia), SDC (samarium-doped ceria), and YSZ/GDC (Yttria-stabilized zirconia/Gadolinium-doped ceria) electrolytes have been constructed using thin-film techniques to overcome the ohmic losses and retain the meaningful fuel cell performance at low temperatures [6–15]. But due to higher cost, difficulty scaling up, and the longer manufacturing time of thin films, these solutions have not been practical for SOFC.

Recently, GDC and other single-layer electrolytes made of semiconductor materials (semiconductor-ionic fuel cell SIFC) have been used to realize fuel cell operation with high ionic conductivity and long-term stability at reduced operational temperature (450–550 °C) [16,17]. For example, Gang-Chen et al. have reported a GDC nanocrystalline electrolyte exhibiting high ionic conductivity of 0.37 S/cm and high fuel cell performance of 591 mW/cm^2 at 550 °C. The amorphous phase in the fuel cell environment with a multitude of O-vacancies at the surface of the GDC was proven to be the primary key for speedy ionic transport via grain boundary diffusion [17]. At the same time, the interfacial conduction in the GDC electrolyte was discovered to be the dominant conduction mechanism for protons and oxide ions. Also, ceria-based electrolytes are a good candidate for delivering high ionic conductivity at intermediate and low operational temperatures. In this regard, the core-shell structure ($CeO_2/CeO_{2-\delta}$) has been reported to build up proton shuttles to obtain higher proton conductivity of 0.16 S/cm and high fuel cell performance of 697 mW/cm^2 at 520 °C. Moreover, non-doped ceria with a primary focus on surface properties of $CeO_{2-\delta}$ has delivered a high ionic conductivity of 0.1 S/cm and a high-power density of 660 mW/cm^2 at low operational temperature. The core-shell structure supported with energy band alignment enhances the ionic conduction while suppressing the electronic conduction [18,19].

The Li-based metal oxide layered structure $Ni_{0.8}Co_{0.15}Al_{0.05}LiO_2$ (NCAL) has commonly been used in semiconductor-based fuel as an efficient electrode, either anode or cathode, due to high catalytic activity and better redox reaction rate at low operational temperature (300–600 °C) [16]. Furthermore, numerous semiconductor and ionic conducting electrolytes (single-phase & heterostructure) have been reported using symmetrical electrodes to perform well at low temperatures. Also, numerous studies have been documented using GDC-based material for higher power density and stability at low (450–550 °C) and intermediate temperatures (500–650 °C) [17,20–23]. However, to our knowledge, there is still no literature on reporting good SOFC performance at exceptionally low operating temperatures, around 350–450 °C.

We report a simple and original design using a GDC electrolyte sandwiched between two symmetrical electrodes (NCAL) under an H_2/Air environment operating at exceptionally low temperatures (350–450 °C). The most known and efficient precipitant agent, Na_2CO_3, synthesized the GDC by employing the co-precipitation method and then used it as the electrolyte in a fuel cell [24]. It delivered a remarkable fuel cell performance of 562 mW/cm^2 and high ionic conductivity at 450 °C. Also, commercial GDC was used as an electrolyte yielding 359 mW/cm^2 at 450 °C. The high performance and better stability at low temperatures are owing to the remaining Na_2CO_3 in the form of a thin layer on the surface of the GDC, which further protects the GDC from being reduced, keeping it stable and creating a rapid interface ionic conduction channel. The obtained results suggest that the surface modification in doped ceria is as essential as in non-doped ceria to enhance the surface functionality in terms of higher fuel cell performance and long-term stability pointing out a different mechanism than in previous reports [17]. The present work provides a new way to design novel electrolytes with high ionic conductivity and better fuel cell performance for advanced and next-generation low-temperature solid oxide fuel cells. The experimental method and results with detailed discussion have been debated in a later section.

Experimental portion

Synthesis of GDC particles

GDC powder was synthesized using the wet chemical co-precipitation method with Na_2CO_3 as a precipitating agent. Typically, 1 g of $Ce(NO_3)_3.6H_2O$ (0.9 g) and $Gd(NO_3)_3.6H_2O$ (0.1 g) (Sigma Aldrich, 99.9%) was dissolved in a beaker of 200 mL deionized water under stirring. Also, the appropriate amount of precipitating agent (Na_2CO_3) was dissolved in a separate beaker of 200 mL of deionized water for mixing. After 4–5 h of stirring, Na_2CO_3 solutions were steadily and dropwise poured into the GDC solution to form fine precipitation. The molar ratio among the GDC and precipitating agent (Na_2CO_3) was 1:2. Afterwards, the mixture solution was stirred for 4 h and then aged for 12 h; subsequently, the final solution was filtered, washed with deionized water to get rid of surface impurities, and dried in an oven at 120 °C calcined in a muffle furnace at 600 °C for 24 and 4 h respectively. In the end, obtained powder was grounded for proper mixing to get a fine powder of GDC. Moreover, the commercial GDC (Ningbo SOFCMAN Energy, Ningbo City, Zhejiang Province, P.R. China) was also used to compare synthesized GDC with Na_2CO_3 precipitating agents. The prepared GDC synthesis procedure and obtained morphology and structure have been shown in Fig. 1.

Fuel cell assembly and measurements

The synthesized and the commercial GDC powder were compressed and sandwiched between two symmetrical electrodes Ni-NCAL ($Ni_{0.8}Co_{0.15}Al_{0.05}LiO_2$). The GDC acts as an electrolyte, whereas the pasted NCAL Ni-foams act as symmetrical electrodes (anode & cathode). The prepared configuration of Ni-NCAL/GDC/NCAL-Ni was compressed under the partial pressure of 250 MPa for 2 min to obtain the circular pellet of button shape with a diameter of 13 mm and an active area of 0.64 cm^2. The thickness of the prepared pellet was 1.5 mm, while the thickness of the electrolyte was 0.75 mm. The prepared cell with the following configuration (Ni-NCAL/GDC/NCAL-Ni) was sintered at 650 for 2 h before the fuel cell measurements. The Ni-NCAL electrode was assembled using commercial NCAL ($Ni_{0.8}Co_{0.15}Al_{0.05}LiO_2$) powders and terpinol solvent. An appropriate amount of terpinol was poured into the NCAL powder to get the viscous slurry of NCAL. At the same time, on the other hand, button-shape Ni-foam was cut with an active area of 0.64 cm^2. Finally, the viscous slurry was pasted on the Ni-foam and then dried at 120 °C for 15 min to form the Ni-NCAL electrode. The remaining detail of the NCAL electrode can be found elsewhere [16].

Later the pellet was fixed into the device to start measuring fuel cell and electrochemical impedance spectroscopy (EIS). At the anode side, fuel was pure hydrogen, and on the cathode side, Air as an oxidant was supplied in 80–120 mL min^{-1} and 150–200 mL $min^{-1,}$ respectively. The fuel cell performance was studied using a programmable electronic load (IT8511) to

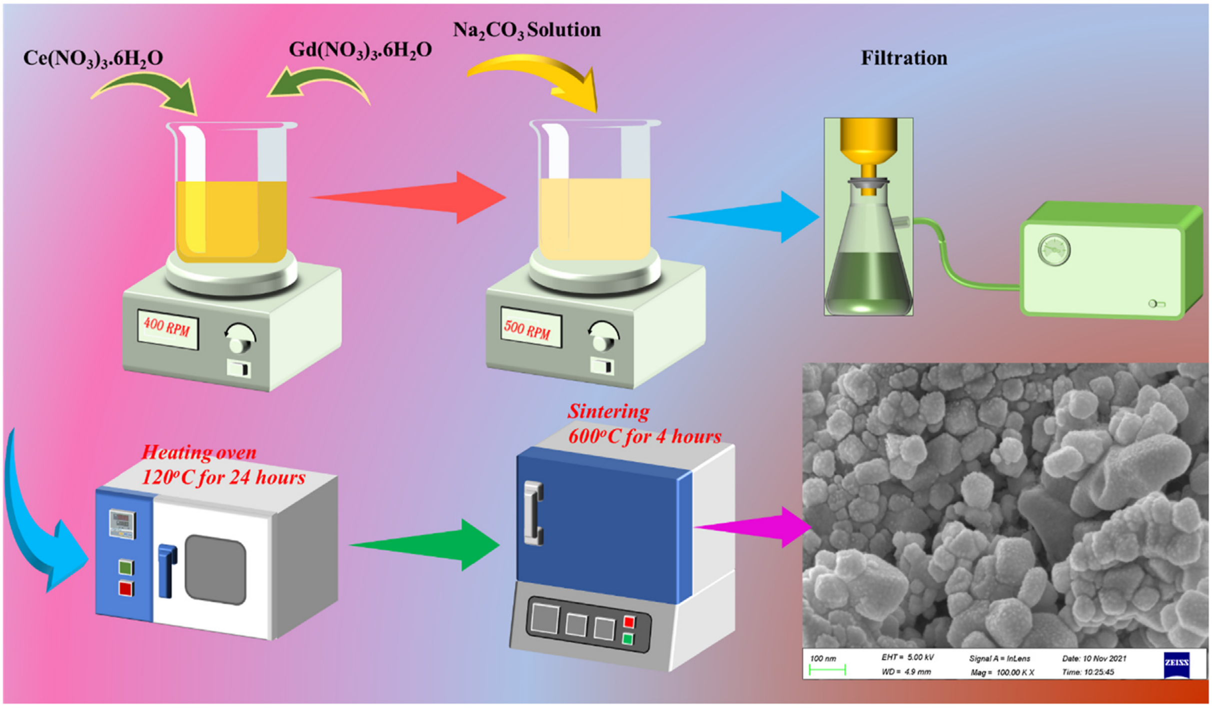

Fig. 1 – Schematic diagram of synthesis procedure of GDC with morphology.

collect the current and voltage reading and plot the I–V/I–P characteristic curve. The Gemmary, 3000 electrochemical workstation was used to measure the electrochemical impedance spectroscopy under H_2/Air environment at different operational temperatures of 350–450 °C. The applied frequency was set in the range of 0.1 Hz–1 MHz with an amplitude of 10 mV.

Characterization

The crystallographic phases were determined and analyzed using the X-ray diffraction (XRD) patterns of the as-synthesized GDC and commercial GDC samples. The XRD analysis was performed using a Bruker D8 X-ray diffractometer (XRD, Germany, Bruker Corporation) under the operating voltage and current of 45 kV and 40 mA, respectively, with Cu Kα radiation ($\lambda = 1.54060$ Å). Field-emission scanning-electron microscope (FESEM, JSM7100F, Japan) was used to analyze the samples operating at 15 kV morphology. A high resolution-transmission electron microscope (HR-TEM, JEOL ARM-200CF) was used to characterize the detailed microstructure further. A 532 nm beam commenced Raman microscope (Lab RAM HR 800 UV, Horiba Jobin Yvon, France) was used to obtain the Raman spectra of commercial and prepared GDC. The thermos gravimetry-differential scanning calorimetry (TG-DSC, NetzschSTA449F5) was used to analyze the thermal weight losses of the powder samples of commercial and prepared GDC, and operation was performed in the temperature range of 29–1200 °C under synthetic air environment. Furthermore, for checking the surface properties of the powder samples of commercial and prepared GDC, X-ray photoelectron spectroscopy (Escalab 250 Xi, Thermo Fisher Scientific, UK) was performed to obtain the XPS spectra.

Results and discussion

Structural and morphological properties of commercial and prepared GDC

In the current study, we have synthesized the GDC electrolyte powder using the wet co-precipitation method. In previous studies, GDC was synthesized with a different methodology to obtain the pure phase of the fluorite structure. The XRD (x-ray diffraction) analysis was used to study the phase of prepared GDC powder. The obtained result have confirmed the formation of pure fluorite structure of GDC, which matched well with the previous studies, as displayed in Fig. 2(a) [17,24].

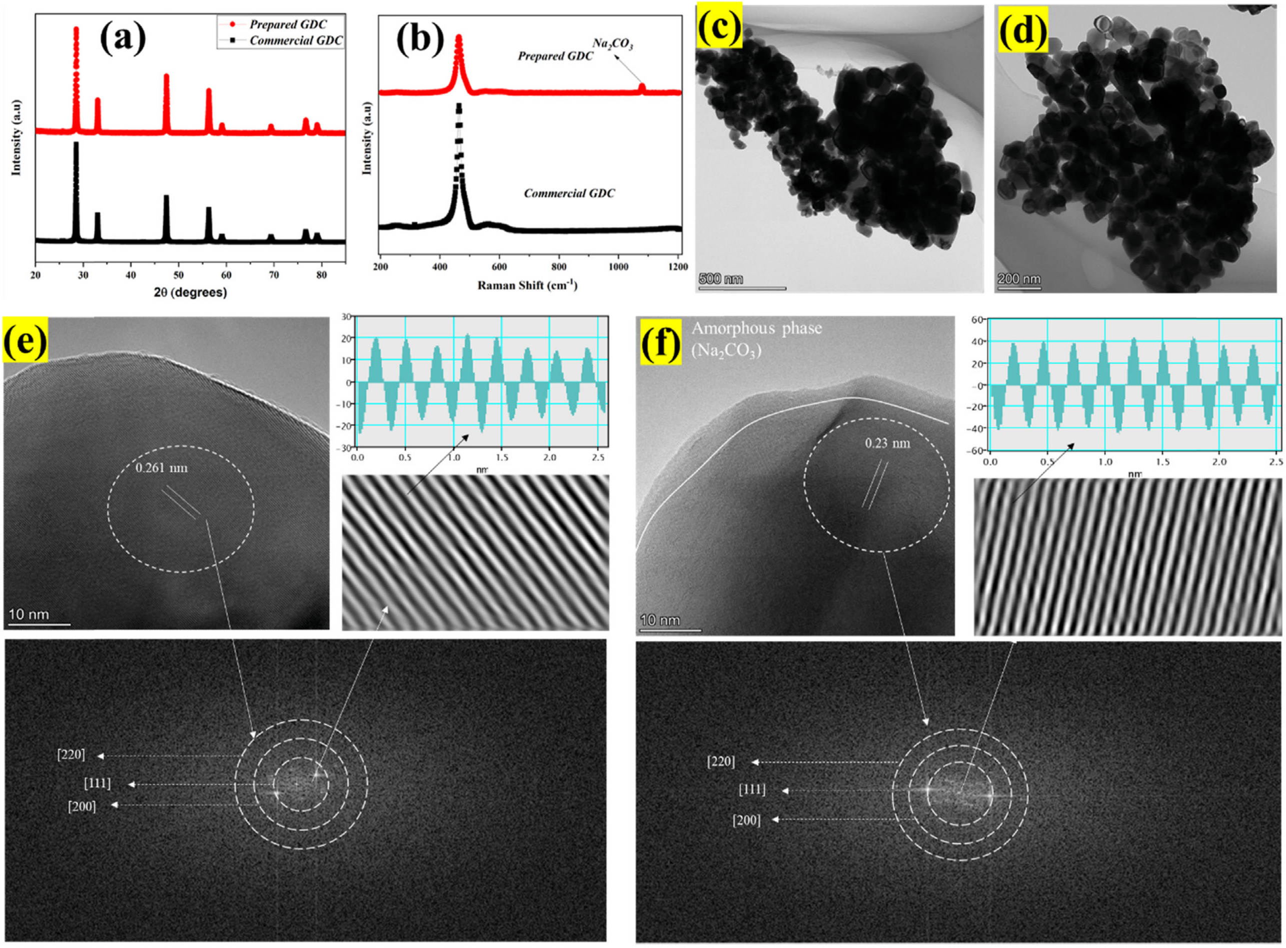

Fig. 2 – (a, b) XRD pattern and Raman spectra of commercial and synthesized GDC (c–f) HR-TEM images of (c, e) commercial and the (d, f) synthesized GDC.

Commercial or synthesized samples have the pure cubic fluorite structure of phase group of Fm3m corresponding to the JCPDS card # 00-034-0394 of refined ceria fluorite structure [18,19]. Both samples show the exact peak positions but slightly different intensities, revealing the GDC fluorite structure. The Scherrer formula was used to calculate the crystalline size of 40 nm and 43 nm corresponding to synthesized and commercial GDC, respectively, confirming nanosized particles' formation. The slight difference in crystalline size might be due to the GDC synthesis using precipitating agent Na_2CO_3 [25].

Raman spectra were performed to investigate further obtained products in both samples (commercial & synthesized GDC), as displayed in Fig. 2(b). Typically, Raman spectra are the most powerful technique to examine the structural properties (local short distance) and defect array in the GDC lattice [25]. The most intense peak in both samples occurred at 468 cm^{-1} due to the F_{2g} symmetric vibration mode of Ce–O bonds, mainly belonging to the CeO_2 fluorite structure. Also, the synthesized sample peak at 1071 cm^{-1} cross ponds to the amorphous phase Na_2CO_3 proves the existence of Na_2CO_3 with no limits in synthesized samples. These findings are well-matched with the previously reported literature [25–29].

Fig. 2(c and d) revealed the HR-TEM image of the commercial GDC and the synthesized GDC exhibiting nanostructure particles, which are homogeneous and well dispersed. The obtained nanostructure is favorable to synergistic effects of GDC particle characteristics, which benefits the electrochemical properties of the prepared device. Moreover, the formation of nanoparticles enhances the surface area. It creates more active sites, benefiting the ionic conductivity of the prepared fuel cell device [25]. Fig. 2(e and f) shows the HR-TEM image at a 10 nm scale with multi fringe [111] with d-spacing of 0.26 nm and 0.23 nm for commercial GDC and synthesized GDC. Also, in synthesized GDC, residual Na_2CO_3 existence has been noticed, confirming the Na_2CO_3 as an amorphous phase covering the GDC surface as a coating layer helps in excelling the ionic transport and protect GDC layers from a reduction in the fuel cell environment [21,25].

Morphological and structural properties

Fig. 3 (a, b) shows the morphology of commercial GDC and synthesized GDC. Both images reveal the uniform distribution of all particles at nanoscale 500 and 100 nm, leading to the

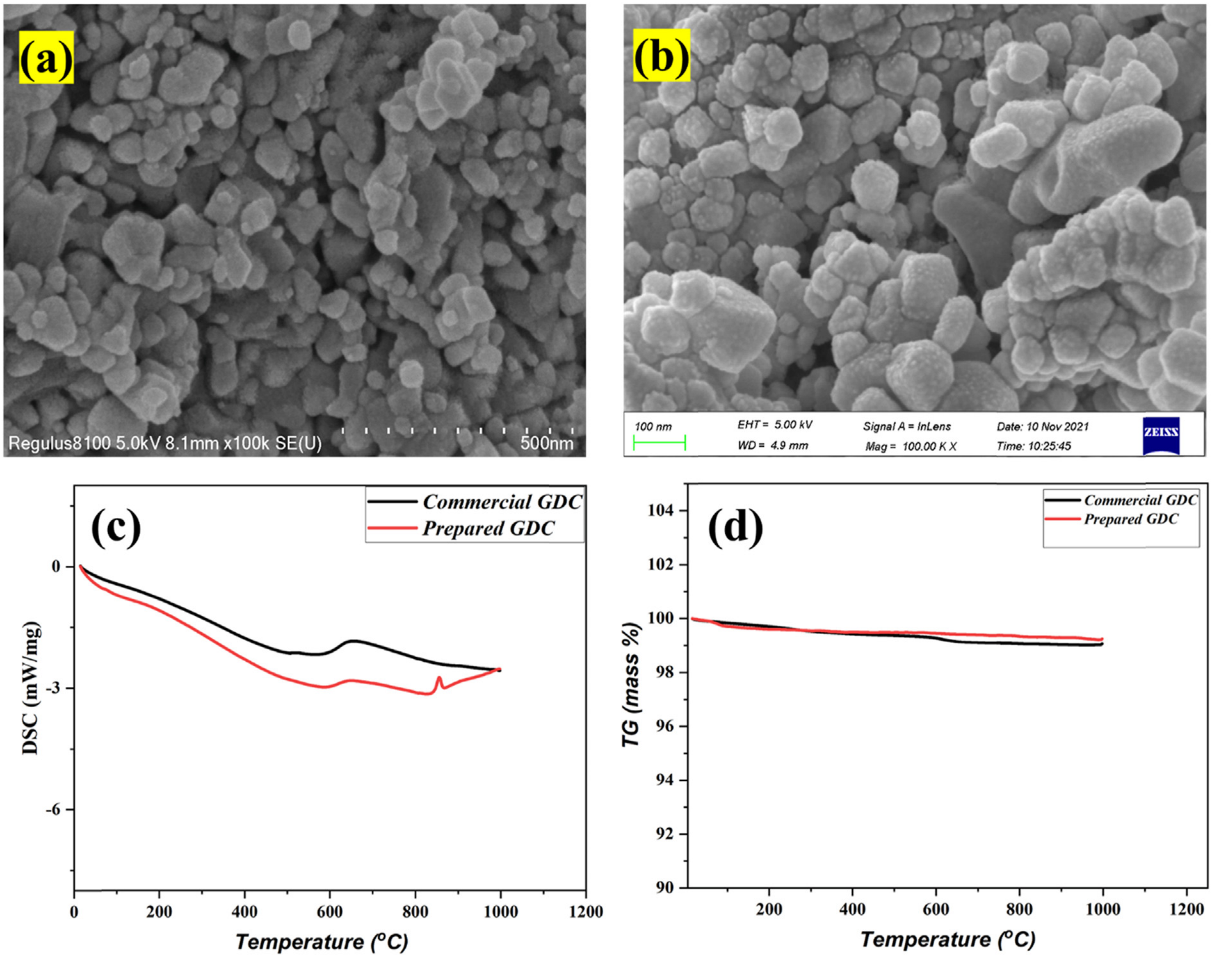

Fig. 3 – a, b) SEM images of commercial and synthesized GDC respectively, c, d) TGA-DSC spectra of commercial and synthesized GDC in the range of 100–1000 °C.

enhanced area and active sites, which benefits the device's electrochemical performance. Both the commercial and synthesized GDC shows a spherical surface; also, the surface of GDC has been covered with Na_2CO_3; the difference can be seen in Fig. 3(a, b).

The commercial, DSC, and TGA characterized the synthesized GDC samples for comparison, as shown in Fig. 3(c and d). DSC and TGA were performed in the temperature range of 30–1200 °C for commercial and synthesized GDC, as depicted separately in Fig. 3(c and d). Two sharp exothermic peaks have been observed in the DSC curve of synthesized GDC, as shown in Fig. 3(c). In contrast, no prominent peak of endothermic or exothermic has been traced in the DSC curve of commercial GDC. The TGA curve for both samples, either the commercial or synthesized GDC, has been displayed in Fig. 3(d). A weight loss of 3–5% has been noticed for synthesized GDC at the temperature range of 68–100 °C, ascribed to the evaporation of absorbed water. Moreover, a slight weight loss was detected in the temperature range of 100–860 °C, possibly due to crystal-absorbed water and moisture resulting in no decomposition reaction. At 850–1000 °C, additional weight loss was noticed, mainly attributed to the melting of Na_2CO_3, as reported earlier [25,30,31]. These results suggest that Na_2CO_3 does not entirely decompose even at high operational temperature, as confirmed by a sharp peak at 858 °C cross-bonds to the Na_2CO_3 in Fig. 3(c).

Surface properties of commercial and prepared GDC

Fig. 4 (a) shows the cropped Ni foam with porous structure, painting of NCAL slurry on Ni foam using the proper brush to cover Ni foam's surface to obtain the Ni-NCAL electrodes (anode & cathode). Fig. 4 (b-d) reveals the SEM image of the porous structure of Ni-foam, the surface of Ni-foam covered NCAL and NCAL particles of prepared electrodes, respectively. The porous structure of Ni -NCAL confirms the better catalytic activity of electrodes and helps enhance the fuel cell device [16]. The SEM image of the porous electrode and cross-sectional view of commercial and prepared GDC pellet have been shown in Fig. SI 1, 2. Moreover, Fig SI.3(a, b) reveals the

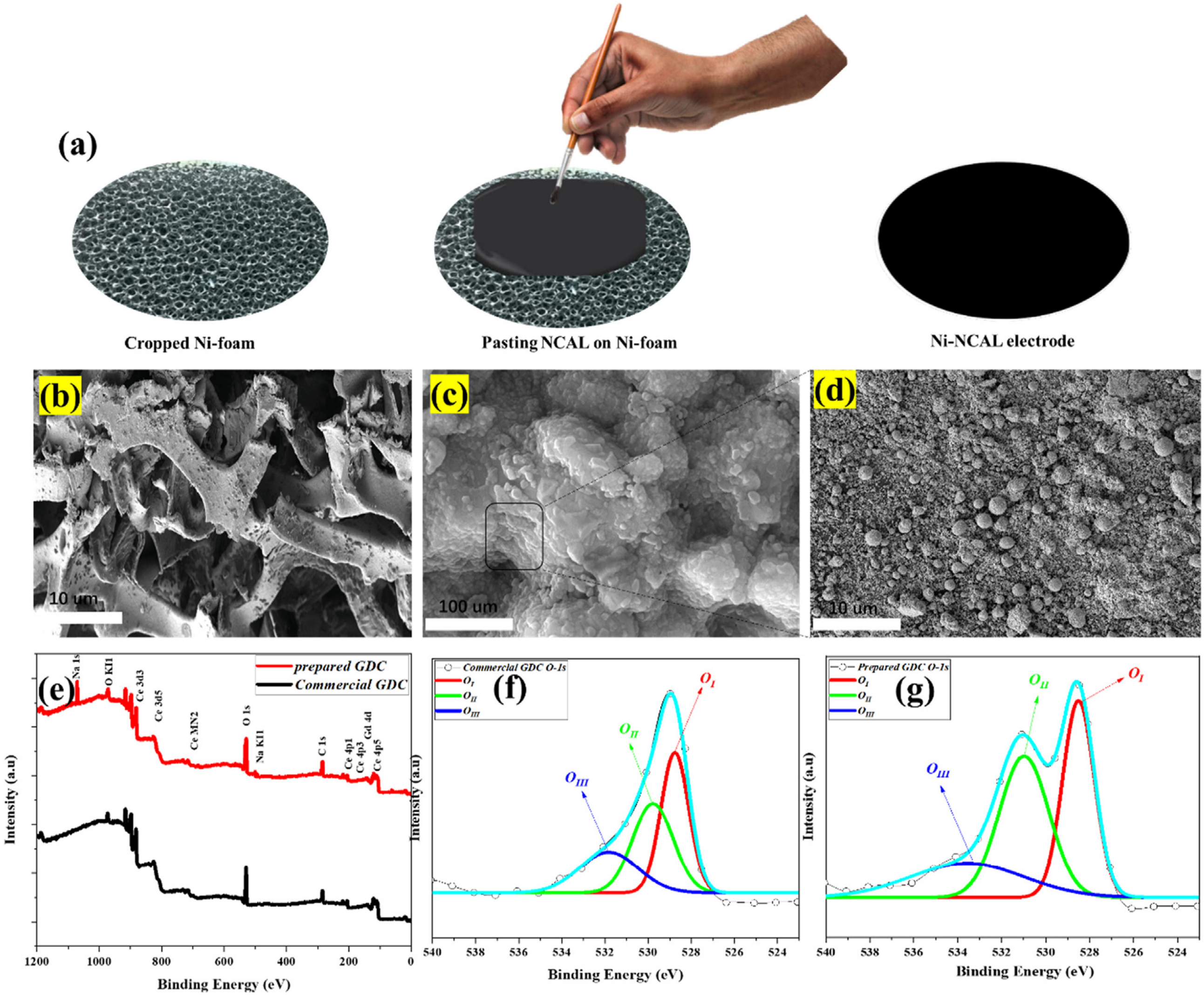

Fig. 4 – a) Schematic diagram of the preparation of Ni-foam pasted NCAL electrodes b-d) SEM of Ni-foam and NCAL electrodes e-g) XPS full spectra and O-1s spectra of commercial and synthesized GDC.

SEM image of commercial and prepared GDC in the μm range (1 μm), showing a clear view of particle connection.

Furthermore, XPS (x-ray photoelectron spectroscopy) analysis was employed to investigate both samples' chemical states (commercial and synthesized GDC). The full XPS spectra of both commercial and synthesized GDC samples have been displayed in Fig. 4(e). A detailed analysis of XPS showed the co-existence of Na, Ce, Gd, and O in synthesized GDC. Most importantly, the sharp peak at the binding energy of 498 eV and 1070 eV indicates the existence of Na in the synthesized GDC lattice. Also, the Ce-3d region is composed of two spin-orbit splits, $3d_{5/2}$ and $3d_{3/2}$ core holes, as demonstrated in Fig. SI 4. Also, the six (v, v^2, v^3, u, $u^{2,}$ and u^3) and four (v^0, v^1, $u^{0,}$ and u^1) fitted peaks of Ce evidenced the presence of two states, Ce^{+4} and $Ce^{+3,}$ respectively, as can be confirmed in the Fig. SI 4(a, b). Also, the obtained peaks and data are well-matched with the previous reports [17,18,32]. The O-1s spectrum of commercial and synthesized GDC have been presented in Fig. 4(f and g). The oxygen spectra of both samples have been deconvoluted into three peaks, O_I, O_{II} and O_{III}. The synthesized materials have widened peak areas which assist in producing more O-vacancies, which might appear due to the usage of precipitating agent Na_2CO_3 in the preparation of GDC. The binding energy 529–530 Ev peak O_I relates to or is connected with the lattice oxygen. While the peak about 531 eV is relevant to O-vacancies and is denoted by O_{II}. The peak at 533 eV can be attributed to surface O-defects or O-species adsorbed on O-vacancies, both of which represent the loosely bound oxygen denoted as O_{III}. Also, it has been speculated that the 528–533 eV peaks signify the existence of oxide ions and O-vacancies, which is essential in enhancing ionic conductivity and impressive electrochemical fuel cell performance [18,19,25,33,34].

Electrochemical fuel cell performance and EIS analysis

The performance of commercial GDC and synthesized GDC electrolytes have been achieved under H_2/Air environments at low operating temperatures of 350–450 °C. The setup of measuring the fuel cell performance, OCV and current density has been displayed in Fig. SI 5. The I–V/I–P characteristics curves of commercial and synthesized GDC are shown in Fig. 5(a and b). The synthesized GDC as electrolyte has delivered meaningful fuel cell performance of 569–237 mW/cm^2 and higher OCV >1V at different and low operating temperatures of 450–350 °C. Moreover, the commercial GDC as an electrolyte also gives good fuel cell performance of 380 mW/cm^2 at 450 °C, but the obtained performance of commercial GDC is less than the synthesized GDC. Also, the received performance of synthesized GDC is higher than the fore-reported electrolyte SFT, SFT-ZnO, CF-LBZY, TiO_2, BCFZY-ZnO, SDC and SDC-STO in SOFCs [34–39].· Such high performance owes to GDC preparation with precipitating agent Na_2CO_3 and low grain boundary resistance, which can be debated in a later section. Moreover, the prepared GDC using Na_2CO_3 as a precipitating agent certainly possess the higher performance due to presence of amorphous layer of Na_2CO_3 leading to enhance the enhance the ionic conduction through surface and interface which eventually increased the fuel cell performance of the prepared device [25,40]. Since we cannot verify that Na_2CO_3 completely covers all GDC particle surface, the characterized "GDC particle/Na_2CO_3 coating layer" unit is not referred to as a core-shell structure in this investigation. Hence, the term "thin coating layer" is more accurate. One thing that the two usual structures have in common is the ability to build a continuous GDC/Na_2CO_3 interface, which has the potential to generate efficient pathways to endow high performance and high ionic conduction. The higher OCV of synthesized and commercial GDC confirms the fuel cell device free of short-circuiting, as shown in Fig. 5(a and b). The commercial GDC has lower OCV than the synthesized GDC, which mainly attributed to the Na_2CO_3 as speculated in previous reports [41,42]. The high voltage and power output have proven the GDC as a feasible and competent electrolyte material, signifying that GDC grasps excellent potential as an electrolyte at exceptionally low temperatures. Such low-temperature performance is also higher than the reported results of a few μ-SOFCs with thin-film electrolytes. For example, YSZ as an electrolyte exhibit 450 mW cm^{-2} at 500 °C and 155 mW cm^{-2} at 510 °C [43,44]. According to the obtained results on one side, the adopted approach has successfully offered a novel and promising technology for LT-SOFC based on GDC electrolytes. At the same time, on the other hand,

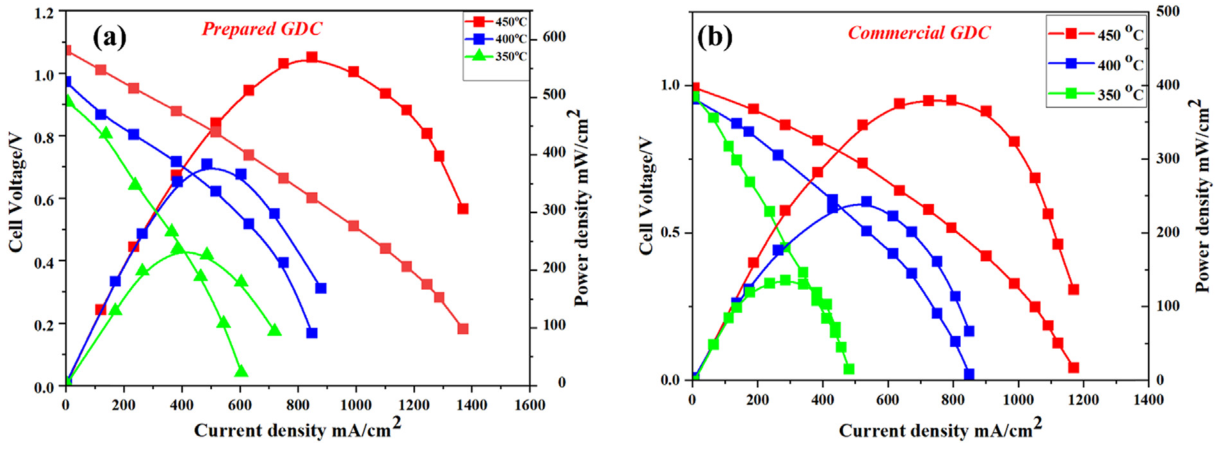

Fig. 5 – a, b) fuel cell performance of synthesized and commercial GDC at (450-350 °C.

more efforts like thin-film techniques and engineering of materials are desperately required to enable it to more advanced technology, especially for LT-SOFCs. Furthermore, the detailed XRD refinement was performed using the full-proof software where the black line signifies the observed value; red represents the calculated one, green shows the difference between the calculated and experimental value and the pink line shows the Bragg position as shown in Fig. SI 3(c). Fig. SI 3(d) shows the comparison graph of the fuel cell performance of commercial and prepared GDC at different operational temperatures 450-350 °C in H_2/Air environment.

To further understand the underlying conductivity, the change of commercial and synthesized GDC nanoparticles has been investigated by employing the impedance spectra of the commercial and synthesized GDC nanoparticles. The constructed fuel cell device was operated under the open-circuit voltage condition at 450 °C in H_2/Air environments, as presented in Fig. 6(a and b). Fig. 6(a and b) presents impedance spectra of synthesized and commercial GDC electrolyte at different operational temperatures of 350–450 °C. The experimental data of EIS were inserted in Z-SIMPWIN software and fitted using the following circuit $LR_o(R_1Q_1)$ (R_2Q_2) (insertion in Fig. 6(a and b) where L, R_o, R_1 and $R_{2,}$ represent the inductance, ohmic, grain boundary and electrode polarization resistance respectively. In contrast, Q represents the constant phase elements depicting a non-ideal capacitor [35,45,46]. The sum of R_1 and R_2 is equal to the polarization resistance ($R_p = R_1+R_2$) where R_p represent the polarization resistance representing the charge as well as the mass transfer resistance. All the simulated parameters have been listed in the supplementary information of Table SI.1. The initial portion at the intercept of higher frequency on the real axis (Z') represents the resistance of grains or bulk resistance R_o. The R_1Q_1 relates to the charge transfer (grain boundary resistance) while the R_2Q_2 relates to electrodes polarization process. The obtained bulk resistance for synthesized and commercial GDC are 0.063, 0.084 and 0.12 Ω-cm^2 and 0.156, 0.44 and 0.84 Ω-cm^2 at 450-350 °C respectively. These lower values of ohmic or bulk resistance are due to presence of abundant number of O-vacancies which eventually enhance the ionic conduction in prepared GDC. Moreover, the obtain resistance of grain boundary (intermediate frequency region) are 0.053, 0.119 and 0.16 Ω-cm^2 and 0.33, 0.63 and 2.02 Ω-cm^2 cross-ponds to the synthesized and commercial GDC at 450-350 °C respectively. The lower value of grain boundary resistance inculcates the creation of more O-vacancies and more ionic conductivity at the surface of GDC.

Moreover, the synthesized GDC has much lower ohmic and grain boundary resistance than the commercial GDC, which

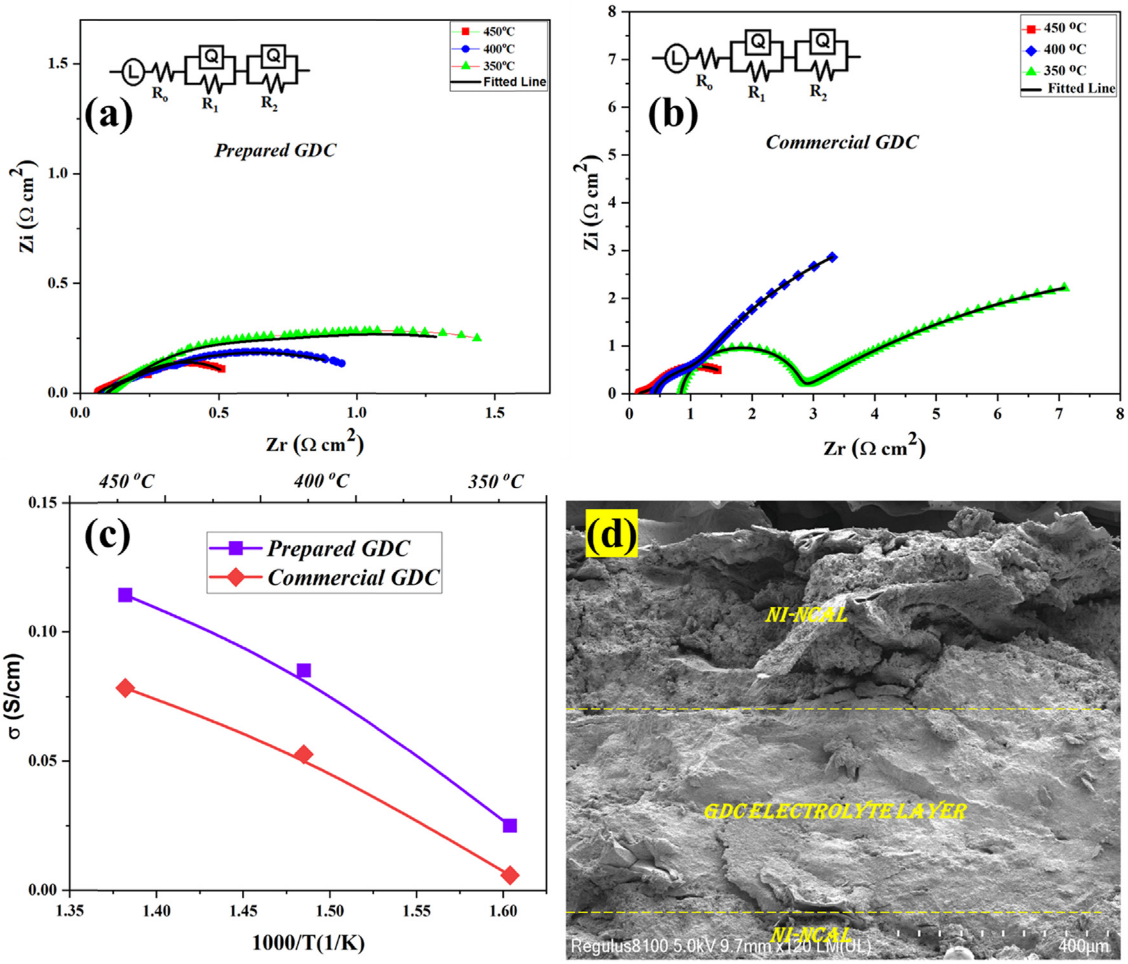

Fig. 6 – a–c) EIS and ionic conductivity of synthesized and commercial GDC at different operational temperatures (450-350 °C) d) shows the cross-sectional view of a cell after fuel cell and EIS measurement.

can be correlated to the remaining Na_2CO_3 at the surface of GDC, which helps in easy transportation of ions, especially grain boundary conduction of GDC [18,19,25,39]. The appearance of GDC can be confirmed in the above results of TEM. Additionally, the electrode polarization resistance was reduced in synthesized GDC and commercial GDC via increasing the temperature 350–450 °C, which manifests thermal effects plays a crucial role in enhancing the performance of fuel cell device. In other hand, NCAL has been pointed out as the best symmetrical electrode resulting in better redox activity even at exceptionally low temperatures of 450–350 °C [16,17].

The lower resistance of bulk and grain boundary signifies higher ionic conductivity. So, to determine the ionic conductivity from the I–V curve, the ohmic resistance was estimated from the central region of the polarization curve, which is further used in the following formula $\sigma = L/R \times A$ where L is the thickness of the electrolyte layer, A is the active area of the pellet [36,38,47–49]. In detail, the total Ohmic polarization losses (V_{ohm}) of the tested cells can be re-created by looking at the linear part of the fuel cell's polarization curve at the low-to-medium current region. This part of the curve is mostly caused by the Ohmic resistance of the electrode and electrolyte. When compared to the ionic resistance of the Prepared

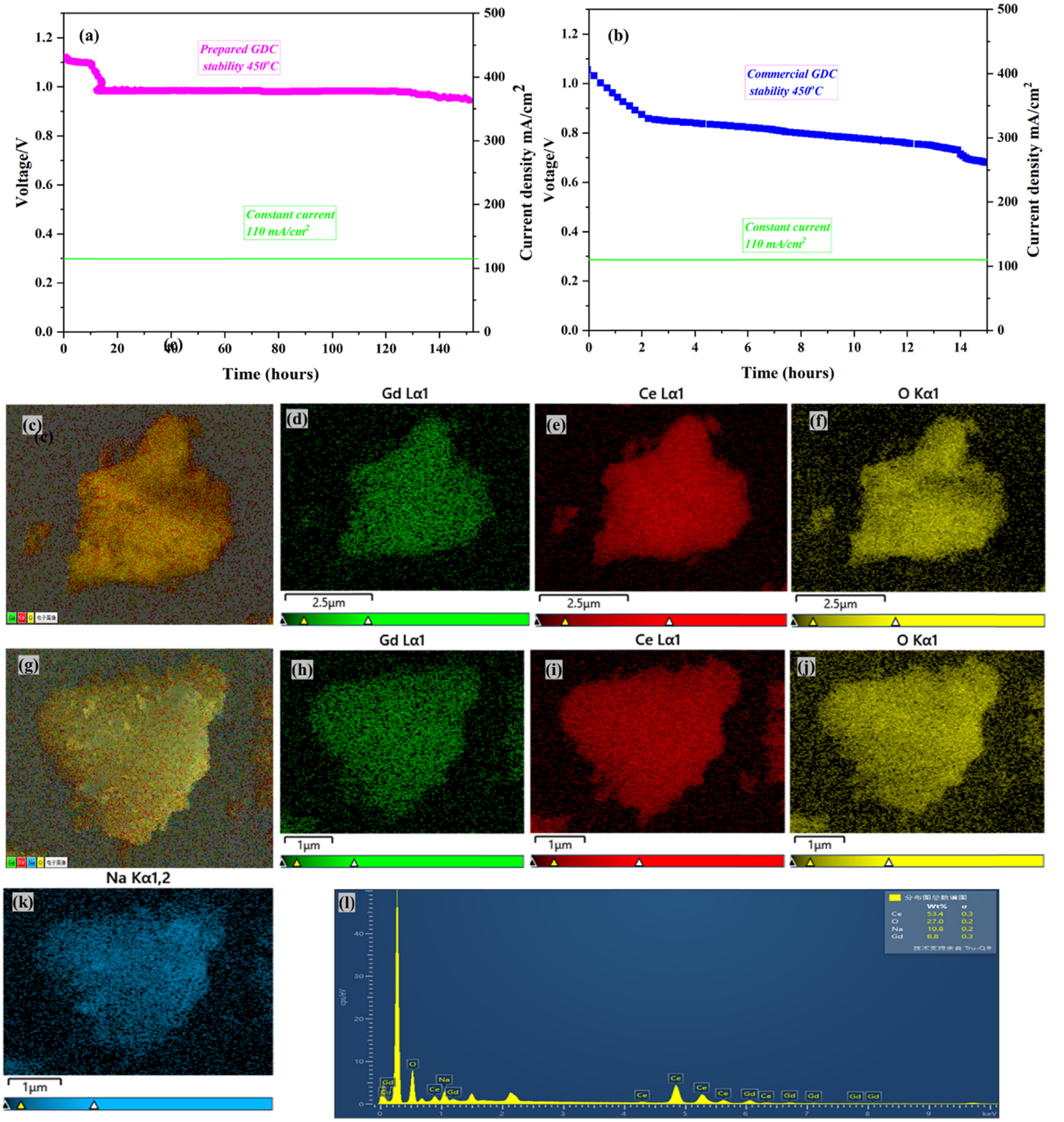

Fig. 7 – a, b) durability operation of synthesized and commercial GDC with a constant current density 110 mA/cm^2 at 450 °C, c-k) the EDS mapping of (c–f) commercial and (g–k) prepared GDC while l) is the elemental mapping of prepared GDC.

GDC electrolyte, the NCAL/Ni-foam electrodes don't offer much in the way of electronic resistance. The total Ohmic resistance from the polarization curve is probably the same as the ionic resistance from the GDC electrolyte that has been made. The ionic conductivity σ_i of synthesized GDC seems fair at an exceptionally low operating temperature of 450 °C. The obtained ionic conductivity of 0.08 S/cm of commercial GDC at 450 °C is lower than the synthesized GDC >0.1 S/cm which might correlate with the Na_2CO_3 as differentiated in Fig. 6(c). Also, attained ionic conduction is bizarrely superior to the reported literature materials SFT, SFT-ZnO, BCFZY-ZnO, SFT-SDC, Li–ZnO, and $LiTiO_3$-LSCF at 450 °C [35,36,38,50–54]. Such high ionic conductivity is believed to be due to surface or grain boundary conduction. Fig. 6(d) shows the cross-sectional view of the prepared cell where electrolyte GDC is sandwiched between two symmetrical porous electrodes NCAL signifying the better OCV and good fuel cell performance, as can be confirmed from the obtained results. Fig. SI 6(a-c) shows the EIS analysis of prepared GDC electrolyte at different operational temperatures 450-350 °C and in different gasses environments H_2 and Air.

The durability of fuel cell device

Furthermore, the durability of commercial and synthesized GDC constructed devices has been investigated at a constant current density of 110 mA/cm^2 under an H_2/Air environment at a low operating temperature of 450 °C, as shown in Fig. 7(a and b). The synthesized GDC stays stable for 150 h. The commercial GDC remains stable for 15 h signifying that the synthesized GDC is more durable than the commercial one. The extended stability proves GDC's feasibility as a competent electrolyte at low operational temperatures. Initially, the cell voltage drops from 1.05 V, which might be due to the activation of electrodes. Still, after 15 h, it gradually reaches a stable point of 0.98 V. That might be due to the enhanced concentration of protons on the surface of GDC, triggering the GDC electrolyte to get the maximum ionic conduction at 450 °C. The long-term durability is also connected with the migration of lithium (Li+) from the electrodes (NCAL) to the electrolyte layer, which creates a stable structural modification between the electrode and electrolyte. The initial few hours of deterioration may also be due to Li + migration toward the electrolyte, until both substances achieve a condition that is compatible [16,55]. After 140 h, a gradual decrease in stability starts due to electrode and electrolyte polarization degradation in synthesized GDC. Also, such long-term stability of the synthesized GDC is owed to the Na_2CO_3, which protects the GDC and helps enable high ionic conductivity. Still, in commercial GDC, continuous degradation phenomena were noticed, which might reduce GDC particles in the H_2 environment, producing electronic conduction and leading to short-circuit as perceived in reported literature [25]. The EDS analysis of commercial GDC, including reference image and all elements like Gd, Ce and O, have been shown in Fig. 7(c–f). Furthermore, the EDS reference image of prepared GDC and all elements such as GD, Ce, O and Na signify that GDC has successfully been prepared with the precipitating agent Na_2CO_3 as confirmed in Fig. 7(g–k). Also, the elemental mapping of prepared GDC has been performed, as shown in Fig. 7(l).

Conclusion

In summary, we designed a GDC-electrolyte with carbonate using the co-precipitation method for use in a fuel cell at an exceptionally low temperature of 350–450 °C. The performance and ionic conductivity of the synthesized GDC are higher than that of a commercial GDC, mainly due to the use of Na_2CO_3 in the preparation phase. The characterization of GDC confirms the existence of Na_2CO_3 in a slight amount on the surface of the GDC particles. The presence of Na_2CO_3 on the surface of GDC reduces the mobility of electrons. It enhances the ionic conduction at the surface and interface, improving the performance of the fuel cell device at low operational temperatures. When the synthesized GDC was applied as an electrolyte in a fuel cell, it delivered a high-power density of 562 mW/cm^2 and a high ionic conductivity of 0.1 S/cm at 450 °C. A tentative durability test of 150 h was very positive due to the inherent protective layer on the GDC. The improvements described here originate from the Na_2CO_3 and the fast grain-boundary ionic conduction on the surface and interfacial conduction. XPS results proved that Synthesized GDC with Na_2CO_3 create more O-vacancy assisting quick kinetics of charges. These results provide new insight into preparing doped ceria to enhance the performance and durability of fuel cell devices at exceptionally low temperatures.

Credit authorship contribution statement

M.A.K. Yousaf Shah: Writing original draft, experimentation, characterization, conceptualization, and methodology. **Yuzheng Lu:** Writing, review, and editing. **Naveed Mushtaq:** Writing, reviewing, and editing. **M. Imran Asghar:** Conceptualization, Writing, review, and editing. **Muhammad Yousaf:** Writing, review, and editing. **Bin Zhu & Peter Lund:** Writing original draft, conceptualization, and methodology.

Declaration of competing interest

The authors declare that they have no known competing financial interests or personal relationships that could have appeared to influence the work reported in this paper.

Acknowledgement

This work was supported by Southeast University (SEU) PROJET # 3203002003A1 and the National Natural Science Foundation of China (NSFC) under the grants # 51772080 and 11604088. Jiangsu Provincial Innovation and Entrepreneurship Talent Program Project No. Dr. Asghar thanks the Hubei Talant 100 programme and Academy of Finland (Grant No. 13329016, 13322738, 13352669) for their financial support.

Appendix A. Supplementary data

Supplementary data to this article can be found online at https://doi.org/10.1016/j.ijhydene.2022.12.314.

REFERENCES

[1] Foger K. The SOFC-XIII satellite seminar. Challenges in commercialization of ceramic fuel cells highly efficient residential generator BlueGen in Europe, vol. 10; 2013. Okinawa.

[2] Singhal S. The SOFC-XIII satellite seminar. SOFC market and commercialization: overview, vol. 10; 2013. Okinawa.

[3] Kordesch KV, Simader GR. Environmental impact of fuel cell technology. Chem Rev 1995;95(1):191–207.

[4] Wachsman ED, Lee KT. Lowering the temperature of solid oxide fuel cells. Science 2011;334(6058):935–9.

[5] Brett DJ, et al. Intermediate temperature solid oxide fuel cells. Chem Soc Rev 2008;37(8):1568–78.

[6] Chen Y-Y, Wei W-CJ. Processing and characterization of ultra-thin yttria-stabilized zirconia (YSZ) electrolytic films for SOFC. Solid State Ionics 2006;177(3–4):351–7.

[7] Huang H, et al. High-performance ultrathin solid oxide fuel cells for low-temperature operation. J Electrochem Soc 2006;154(1):B20.

[8] Shim JH, et al. Atomic layer deposition of yttria-stabilized zirconia for solid oxide fuel cells. Chem Mater 2007;19(15):3850–4.

[9] Kerman K, Lai BK, Ramanathan S. Nanoscale compositionally graded thin-film electrolyte membranes for low-temperature solid oxide fuel cells. Adv Energy Mater 2012;2(6):656–61.

[10] Takagi Y, et al. Low temperature thin film solid oxide fuel cells with nanoporous ruthenium anodes for direct methane operation. Energy Environ Sci 2011;4(9):3473–8.

[11] Tsuchiya M, Lai B-K, Ramanathan S. Scalable nanostructured membranes for solid-oxide fuel cells. Nat Nanotechnol 2011;6(5):282–6.

[12] Kerman K, Lai B-K, Ramanathan S. Pt/Y0. 16Zr0. 84O1. 92/Pt thin film solid oxide fuel cells: electrode microstructure and stability considerations. J Power Sources 2011;196(5):2608–14.

[13] Su P-C, et al. Solid oxide fuel cell with corrugated thin film electrolyte. Nano Lett 2008;8(8):2289–92.

[14] Garbayo I, et al. Full ceramic micro solid oxide fuel cells: towards more reliable MEMS power generators operating at high temperatures. Energy Environ Sci 2014;7(11):3617–29.

[15] Rivera A, Santamarıa J, Leon C. Electrical conductivity relaxation in thin-film yttria-stabilized zirconia. Appl Phys Lett 2001;78(5):610–2.

[16] Chen G, et al. Investigation of layered Ni0. 8Co0. 15Al0. 05LiO2 in electrode for low-temperature solid oxide fuel cells. Int J Hydrog Energy 2018;43(1):417–25.

[17] Chen G, et al. Advanced fuel cell based on new nanocrystalline structure Gd0. 1Ce0. 9O2 electrolyte. ACS Appl Mater Interfaces 2019;11(11):10642–50.

[18] Xing Y, et al. Proton shuttles in CeO2/CeO2− δ core–shell structure. ACS Energy Lett 2019;4(11):2601–7.

[19] Wang B, et al. Fast ionic conduction in semiconductor CeO2-δ electrolyte fuel cells. NPG Asia Mater 2019;11(1):1–12.

[20] Lee W, et al. Oxygen surface exchange at grain boundaries of oxide ion conductors. Adv Funct Mater 2012;22(5):965–71.

[21] Lee JG, Park JH, Shul YG. Tailoring gadolinium-doped ceria-based solid oxide fuel cells to achieve 2 W cm− 2 at 550 C. Nat Commun 2014;5(1):1–10.

[22] Ge L, et al. Boosting the performance of conventional air electrodes for solid oxide cells by in-situ loading of nano praseodymium oxide. Energy Convers Manag 2021;249:114873.

[23] Shin JF, et al. Self-assembled dynamic perovskite composite cathodes for intermediate temperature solid oxide fuel cells. Nat Energy 2017;2(3):1–7.

[24] Raza R, et al. Improved ceria–carbonate composite electrolytes. Int J Hydrog Energy 2010;35(7):2684–8.

[25] Akbar M, et al. High-performing and stable non-doped ceria electrolyte with amorphous carbonate coating layer for low-temperature solid oxide fuel cells. Electrochim Acta 2021;393:139067.

[26] Akbar M, et al. Insights on the interfacial processes involved in the mechanical and redox stability of the BaCe0. 65Zr0. 20Y0. 15O3− δ–Ce0. 85Gd0. 15O2− δ composite. ACS Appl Energy Mater 2020;3(10):9877–88.

[27] Deus R, et al. Influence of mineralizer agents on the growth of crystalline CeO2 nanospheres by the microwave-hydrothermal method. J Alloys Compd 2013;550:245–51.

[28] Huang Y, et al. Bifunctional catalytic material: an ultrastable and high-performance surface defect CeO2 nanosheets for formaldehyde thermal oxidation and photocatalytic oxidation. Appl Catal B Environ 2016;181:779–87.

[29] Li C, et al. Processing temperature tuned interfacial microstructure and protonic and oxide ionic conductivities of well-sintered Sm0. 2Ce0. 8O1. 9-Na2CO3 nanocomposite electrolytes for intermediate temperature solid oxide fuel cells. J Power Sources 2017;360:114–23.

[30] Yin S, et al. Investigation of Sm0. 2Ce0. 8O1. 9/Na2CO3 nanocomposite electrolytes: preparation, interfacial microstructures, and ionic conductivities. ACS Appl Mater Interfaces 2013;5(24):12876–86.

[31] Ma Y, et al. Thermal stability study of SDC/Na2CO3 nanocomposite electrolyte for low-temperature SOFCs. Int J Hydrogen Energy 2010;35(7):2580–5.

[32] Li Y, et al. Enhanced potassium-ion storage of the 3d carbon superstructure by manipulating the nitrogen-doped species and morphology. Nano-Micro Lett 2021;13(1):1–14.

[33] Wang F, et al. Surface-engineered homostructure for enhancing proton transport. Small Methods 2022;6(1):2100901.

[34] Dong W, et al. Semiconductor TiO 2 thin film as an electrolyte for fuel cells. J Mater Chem 2019;7(28):16728–34.

[35] Shah MY, et al. Demonstrating the potential of iron-doped strontium titanate electrolyte with high-performance for low temperature ceramic fuel cells. Renew Energy 2022;196:901–11.

[36] Shah MAKY, et al. The semiconductor SrFe0. 2Ti0. 8O3-δ-ZnO heterostructure electrolyte fuel cells. Int J Hydrog Energy 2019;44(57):30319–27.

[37] Shah MY, et al. Novel perovskite semiconductor based on Co/Fe-Codoped LBZY (La0. 5Ba0. 5 Co0. 2Fe0. 2Zr0. 3Y0. 3O3− δ) as an electrolyte in ceramic fuel cells. ACS Appl Energy Mater 2021;4(6):5798–808.

[38] Xia C, et al. Shaping triple-conducting semiconductor BaCo0. 4Fe0. 4Zr0. 1Y0. 1O3-δ into an electrolyte for low-temperature solid oxide fuel cells. Nat Commun 2019;10(1):1–9.

[39] Cai Y, et al. A bulk-heterostructure nanocomposite electrolyte of Ce0. 8Sm0. 2O2-δ–SrTiO3 for low-temperature solid oxide fuel cells. Nano-Micro Lett 2021;13(1):1–14.

[40] Wang X, et al. Novel core–shell SDC/amorphous Na2CO3 nanocomposite electrolyte for low-temperature SOFCs. Electrochem Commun 2008;10(10):1617–20.

[41] Huang J, et al. Development of novel low-temperature SOFCs with co-ionic conducting SDC-carbonate composite electrolytes. Electrochem Commun 2007;9(10):2601–5.

[42] Zhou X, et al. Improving grain boundary conductivity of Ce0. 9Gd0. 1O2− δ electrolyte through compositing with carbonate or semiconductor. Energy Technol 2020;8(9):2000424.

[43] Sajid A, et al. A perspective on development of fuel cell materials: electrodes and electrolyte. Int J Energy Res 2022;46(6):6953–88.

[44] Nahak BK, et al. Metal oxide nanostructured materials for photocatalytic hydrogen generation. In: Emerging nanomaterials for advanced technologies. Springer; 2022. p. 665–708.

[45] Rauf S, et al. Application of a triple-conducting heterostructure electrolyte of Ba0. 5Sr0. 5Co0. 1Fe0. 7Zr0. 1Y0. 1O3− δ and Ca0. 04Ce0. 80Sm0. 16O2− δ in a high-performance low-temperature solid oxide fuel cell. ACS Appl Mater Interfaces 2020;12(31):35071–80.

[46] Shah MY, et al. Perovskite Al-SrTiO 3 semiconductor electrolyte with superionic conduction in ceramic fuel cells. Sustainable Energy & Fuels; 2022.

[47] Mushtaq N, et al. Promoted electrocatalytic activity and ionic transport simultaneously in dual functional Ba0. 5Sr0. 5Fe0. 8Sb0. 2O3-δ-Sm0. 2Ce0. 8O2-δ heterostructure. Appl Catal B Environ 2021;298:120503.

[48] Shah MY, et al. Advanced fuel cell based on semiconductor perovskite La–BaZrYO3-δ as an electrolyte material operating at low temperature 550° C. Int J Hydrog Energy 2020;45(51):27501–9.

[49] Shah MY, et al. Electrochemical properties of a co-doped SrSnO3− δ-based semiconductor as an electrolyte for solid oxide fuel cells. ACS Appl Energy Mater 2020;3(7):6323–33.

[50] Shah MY, et al. Semiconductor Fe-doped SrTiO3-δ perovskite electrolyte for low-temperature solid oxide fuel cell (LT-SOFC) operating below 520° C. Int J Hydrog Energy 2020;45(28):14470–9.

[51] Mushtaq N, et al. Tuning the energy band structure at interfaces of the SrFe0. 75Ti0. 25O3− δ–Sm0. 25Ce0. 75O2− δ heterostructure for fast ionic transport. ACS Appl Mater Interfaces 2019;11(42):38737–45.

[52] Xia C, et al. Semiconductor electrolyte for low-operating-temperature solid oxide fuel cell: Li-doped ZnO. Int J Hydrog Energy 2018;43(28):12825–34.

[53] Shah MY, et al. ZnO/MgZnO heterostructure membrane with type II band alignment for ceramic fuel cells. 2022.

[54] Wang F, et al. Li2TiO3–LaSrCoFeO3 semiconductor heterostructure for low temperature ceramic fuel cell electrolyte. Int J Hydrog Energy 2021;46(24):13265–72.

[55] Wei K, et al. Ionic conduction of ceramic/molten salt composite electrolyte in fuel cell with lithium compound as electrode. J Electrochem Soc 2022;169(9):094503.